Hindawi Publishing Corporation
Journal of Geological Research
Volume 2014, Article ID 582424, 12 pages
http://dx.doi.org/10.1155/2014/582424

Research Article

Indications for the Occurrence of Gas Hydrates in the Fram Strait from Heat Flow and Multichannel Seismic Reflection Data

W. H. Geissler,[1] P. V. Pulm,[2] W. Jokat,[1] and A. C. Gebhardt[1]

[1] *Alfred-Wegener-Institut Helmholtz-Zentrum für Polar- und Meeresforschung, Am Alten Hafen 26, 27568 Bremerhaven, Germany*
[2] *Q-con GmbH, Marktstraße 39, 76887 Bad Bergzabern, Germany*

Correspondence should be addressed to W. H. Geissler; wolfram.geissler@awi.de

Received 26 September 2013; Revised 10 December 2013; Accepted 23 December 2013; Published 9 February 2014

Academic Editor: Michela Giustiniani

The distribution of gas hydrates recently raised increased attention, especially along glaciated continental margins, due to its potential importance for slope stability and global climate. We present new heat flow data together with multichannel reflection seismic data from the central Fram Strait in-between Northeast Greenland and Svalbard. This area is only accessible by icebreaking vessels, and, therefore, knowledge about this area is still sparse. The new heat flow data concur with previous measurements in the region. High temperature gradients of >200 mK/m were recorded along the active spreading zone in the Fram Strait, and gradients of 75 mK/m along the western slope of Yermak Plateau. Along the Northeast Greenland slope, the measured gradients reach 54 mK/m at maximum. Seismic data image bottom-simulating reflections proofing that the known gas-hydrate province spreads much further north along the western slope of the Yermak Plateau than previously known. Existing slide scars indicate that there might be a causal relationship between the occurrence of gas hydrates and slope instability in that area. Along the Northeast Greenland continental margin and in the adjacent abyssal plain, strong indications for the occurrence of gas within the sedimentary basins and for its migration along fault zones and chimney-like structures are found.

1. Introduction

During the last years the scientific interest on gas hydrates and their worldwide occurrences constantly grew. As pointed out, for example, by Tinivella and Giustiniani [1], the understanding of gas hydrates, their stability, and relationship to overpressure conditions at its base, water depth, and geothermal gradient are very important, not only in the aspects of hazard potential. Gas hydrates are an ice-like substrate consisting of light hydrocarbons (mostly methane), which are trapped in the lattice of water molecules [2]. They occur all over the world at both rifted and active margin settings. In high pressure and low temperature conditions gas hydrates exist within the sediments pore space. They are stable in the upper sediment layers where those requirements are met, within the gas hydrate stability zone (GHSZ). Gas hydrates along glaciated margins might react extremely sensitive to changes in bottom-water temperatures and, therefore, climate change [3]. They represent a significant geohazard, because their occurrence is closely linked to slope stability [4]. The northern continental rifted margin of Svalbard exhibits one of the largest slope failures on the globe (e.g., [5]). However, up to now it is not clear if gas hydrates and their potential dissolution played a major role during the slide event [5, 6]. Furthermore, the escape of methane may contribute to methane anomalies in the atmosphere as discussed, for example, in Hustoft et al. [7] and Gentz et al. [8].

If methane hydrates destabilize, the gas phase emanates in the water column in the form of bubble plumes, which can be detected with high resolution hydroacoustic sensors in the water column [9]. Indications for gas hydrates and free gas at the south-western Svalbard continental margin were first observed by Vogt et al. [10]. Hustoft et al. [7] studied a pockmark field at Vestnesa (Figure 1) that shows active venting presumably due to gas overpressure beneath the gas hydrate stability zone. Increase in bottom water temperature might have caused a decrease of GHSZ thickness and therefore a lateral shift of the GHSZ position along

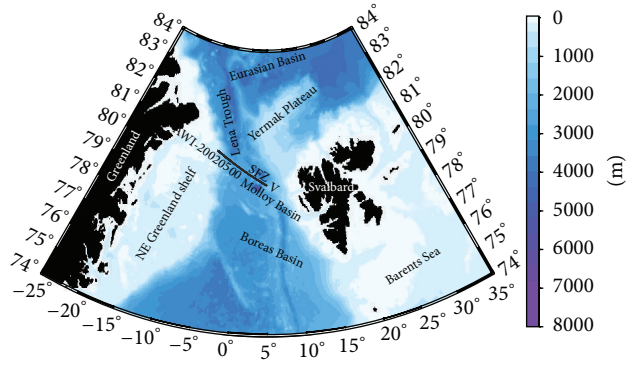

FIGURE 1: Overview over the study area. SFZ, Spitsbergen Fracture Zone; V, Vestnesa.

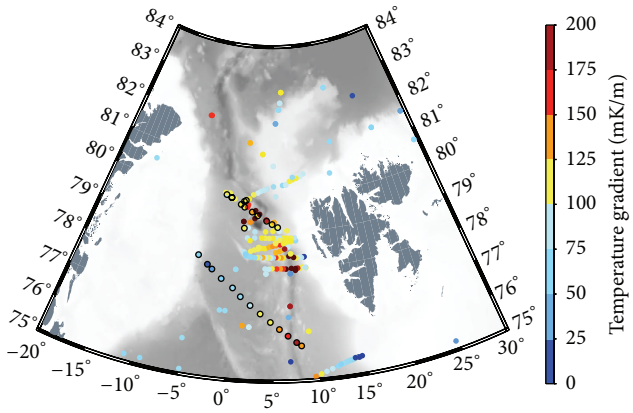

FIGURE 2: Heat flow temperature gradients in the Fram Strait. Unrimmed data points are taken from IHFC and University of Oslo databases. The black-rimmed data points are measured during ARK XXIV/3. A detailed station list is presented in Table 1. The IBCAO bathymetry is underlain like in all other figures.

the western Svalbard continental margin and finally led to an increase in methane gas venting [11]. In this case, the line in which the phase boundary between free gas and gas hydrates intersects the sea floor moves downslope. The intersection between the base of the GHSZ and the seafloor is the most sensitive zone to oceanographic or climate changes, because this zone is more affected by changes in bottom water temperatures than layers deeper beneath the seafloor [1, 12].

The equilibrium of methane hydrates depends on several parameters. The most important ones are temperature and pressure, respectively, water depth [2]. The gas hydrate is stable, as long as the temperature is lower than the temperature of the gas hydrate phase boundary for a certain depth. The depth of the gas hydrate boundary increases with water depth/pressure, while the real temperature first decreases in the water column and then increases in the sediment again [2, 13]. Gas hydrate occurrence is strongly related to temperature. Thus, heat flow data can be used for a prediction of the thickness of the GHSZ [14].

In seismic reflection data, the lower boundary of the GHSZ can often easily be recognised by a bottom-simulating reflector (BSR), a reflector which follows the seafloor topography. It represents the boundary between gas hydrates and free gas [7, 15]. In the gas-filled zone, if there is any below the hydrates, P-wave velocities decrease [16, 17]. The most typical characteristic of the BSR is a phase reversal due to a negative acoustic impedance at the boundary between hydrates and free gas. If there is no BSR in turn, hydrates are not necessarily absent.

In this study we combine existing multichannel seismic reflection data with new and published heat flow data to evaluate the occurrence of gas hydrates along the western slope of the Yermak Plateau and along the Northeast Greenland continental margin. With our new findings it becomes clear that the known gas hydrate province west of Svalbard extends much further northwards into the northern Fram Strait.

2. Materials and Methods

A global heat flow database (IHFC) was compiled by Pollack et al. [18]. It consists of 24,420 heat flow values on land as well as on sea [19]. A supplementary dataset for heat flow data in the study area was provided by the University of Oslo (UiO) (see [20] and references therein). Data points from the global heat flow database as well as from UiO are mainly excerpts from publications. Some of them just contain values for the temperature gradient, and others also list thermal conductivity and heat flow (Figure 2).

New heat flow data for the Greenland Sea and East Greenland continental margin were gathered in 2009 on board R/V POLARSTERN during expedition ARK-XXIV/3 [21]. The heat flow profiles north of 75°N (Figure 2) were acquired along existing multichannel seismic reflection lines [22, 23] and along a seismic refraction line acquired in 2009 [24]. During the ARK-XXIV/3 expedition, the geothermal gradient was measured with a 8 m long probe that holds 21 temperature sensors with a spacing of 0.27 m. In most cases, measurements were carried out twice at each station. The probe was lowered through the water column down to 100 m above seafloor. Once the sensor temperatures became constant, the probe was lowered into the sediment at 0.8 m/s. After 7 to 10 minutes, when the disturbances in temperature due to friction disappeared and the signal became stable, the probe was pulled out at 0.2 m/s.

Processing of the heat flow measurements was carried out using an improved version of the HFRED software [25] assuming an asymptotic solution for the temperature decay function. A fixed conductivity of 1 W/mK was used, which is a rough mean of measured thermal conductivities from the North Atlantic and Arctic Ocean [20, 26]. For bottom water temperatures, average temperatures measured along a mooring line at 79°N [27] were taken: 275 Kelvin (2°C) at water depths <500 m, 274 Kelvin (1°C) at water depths of 500 to 1000 m, and 272 Kelvin (−1°C) at water depths >1000 m.

Multichannel seismic reflection profiles used in this study were acquired within sea ice covered areas using icebreaker R/V POLARSTERN in 2002 and 2004 [23, 30–32]. A 24-l airgun array and a 600-m-long streamer (96 channels, 6.25 m group spacing) were used to gather the seismic data. All data

Table 1: Heat flow data gathered in 2009 (Jokat, 2010 [21]).

Station	Station name, on board	Heat flow station name	Latitude	Longitude	Water depth [m]	Heat flow [mW/m^2]
HF5	PS74/255	—	80.290	−5.584	792	n.c.p.
HF6	PS74/256	—	80.232	−4.837	—	n.p.
HF7	PS74/257	—	80.145	−4.013	2145	n.p.
HF8	PS74/258	—	80.085	−3.145	2537	n.p.
HF9-1	PS74/259	H0937P01	79.945	−2.129	2713	83
HF9-2	PS74/259	H0937P02	79.945	−2.129	2727	84
HF10-1	PS74/260	H0938	79.881	−1.315	2770	95
HF10-2	PS74/260	H0939	79.883	−1.280	2772	93
HF11-1	PS74/261	H0940	79.840	−0.949	2742	105
HF11-2	PS74/261	H0941	79.840	−0.949	2742	103
HF12	PS74/262	H0942	79.809	−0.667	2750	116
HF13-1	PS74/263	H0943P01	79.717	0.223	2765	116
HF13-2	PS74/263	H0943P02	79.720	0.209	2765	115
HF14-1	PS74/264	H0944P01	79.652	0.770	2605	108
HF14-2	PS74/264	H0944P02	79.652	0.770	2605	104
HF15-1	PS74/265	H0945P01	79.531	1.946	2726	136
HF15-2	PS74/265	H0945P02	79.531	1.946	2726	143
HF16-1	PS74/266	H0946P01	79.434	2.792	2660	118
HF16-2	PS74/266	H0946P02	79.434	2.792	2660	121
HF17-1	PS74/267	H0947P01	79.297	4.119	2520	141
HF17-2	PS74/267	H0947P02	79.297	4.119	2520	138
HF18-1	PS74/268	H0948P01	79.208	4.917	1556	118
HF18-2	PS74/268	H0948P02	79.208	4.917	1556	118
HF19-1	PS74/269	H0949P01	79.125	5.715	1278	104
HF19-2	PS74/269	H0949P02	79.125	5.715	1280	97
HF20-1	PS74/270	H0950P01	78.219	−4.876	969	54
HF20-2	PS74/270	H0950P02	78.219	−4.876	976	56
HF21	PS74/271	—	78.104	−4.234	2245	n.p.
HF22-1	PS74/272	H0951P01	78.000	−3.537	2685	20
HF22-2	PS74/272	H0951P02	78.000	−3.537	2685	21
HF23-1	PS74/273	H0952P01	77.890	−2.869	2835	35
HF23-2	PS74/273	H0952P02	77.890	−2.869	2835	36
HF24-1	PS74/274	H0953P01	77.666	−1.531	3012	52
HF24-2	PS74/274	H0953P02	77.666	−1.531	3014	50
HF25-1	PS74/276	H0954P01	77.445	−0.238	3131	66
HF25-2	PS74/276	H0954P02	77.445	−0.238	3120	65
HF26-1	PS74/278	H0955P01	77.223	1.041	3184	64
HF26-2	PS74/278	H0955P02	77.223	1.041	3182	64
HF27-1	PS74/280	H0956P01	77.002	2.283	3201	83
HF27-2	PS74/280	H0956P02	77.002	2.283	3201	80
HF28-1	PS74/282	H0957P01	76.781	3.527	3220	101
HF28-2	PS74/282	H0957P02	76.781	3.527	3217	101
HF29-1	PS74/284	H0958P01	76.557	4.738	3000	107
HF29-2	PS74/284	H0958P02	76.557	4.738	2997	104
HF30-1	PS74/286	H0959P01	76.365	5.767	2615	144
HF30-2	PS74/286	H0959P02	76.365	5.767	2615	144
HF31-1	PS74/288	H0960P01	76.182	6.742	2526	170
HF31-2	PS74/288	H0960P02	76.182	6.742	2525	172
HF32-1	PS74/290	H0961P01	76.004	7.684	2665	189
HF32-2	PS74/290	H0961P02	76.004	7.684	2665	189
HF33-1	PS74/291	H0962P01	75.903	8.217	2279	140
HF33-2	PS74/291	H0962P02	75.903	8.217	2276	142

n.c.p: no complete penetration; n.p.: no penetration.

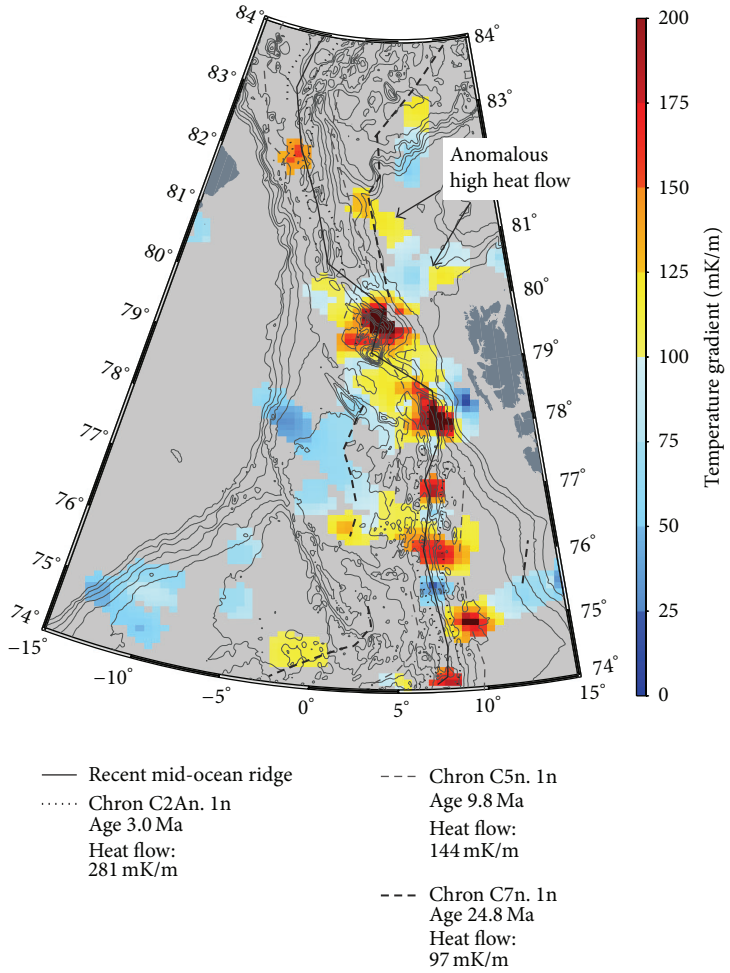

Figure 3: Distribution of temperature gradient in context with ages of magnetic anomalies after Engen et al. [28]. The theoretical heat flow for the magnetic chrons was calculated according to (1). Contour line spacing of isobaths is 500 m.

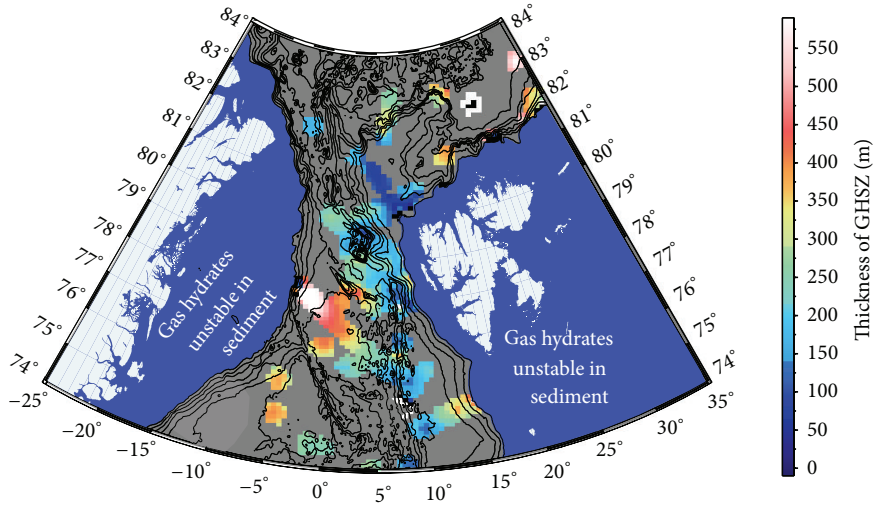

Figure 4: Predicted thickness of GHSZ (m), grid spacing 10 km. The blue areas are those where no gas hydrates are stable in the sediments.

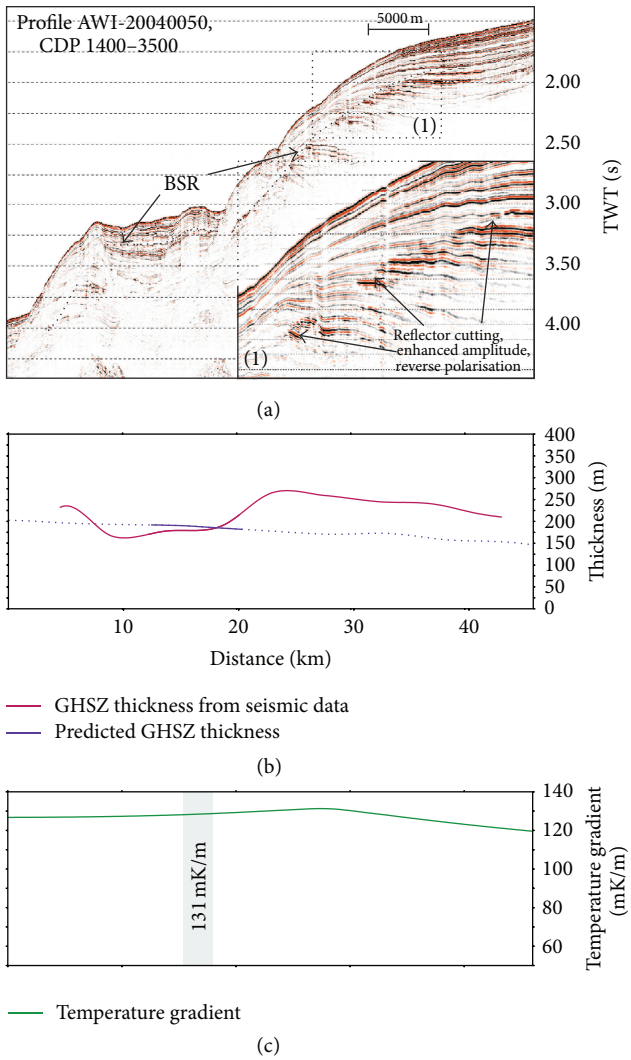

Figure 5: (a) Seismic profile AWI-20040050 (see Figure 8 for location) with BSR. Inset (1) shows the BSR. (b) Interpolated GHSZ thickness along this profile is shown in pink and predicted GHSZ thickness is shown in violet. (c) Interpolated temperature gradient along this profile, grey boxes indicate heat flow measurements on that profile.

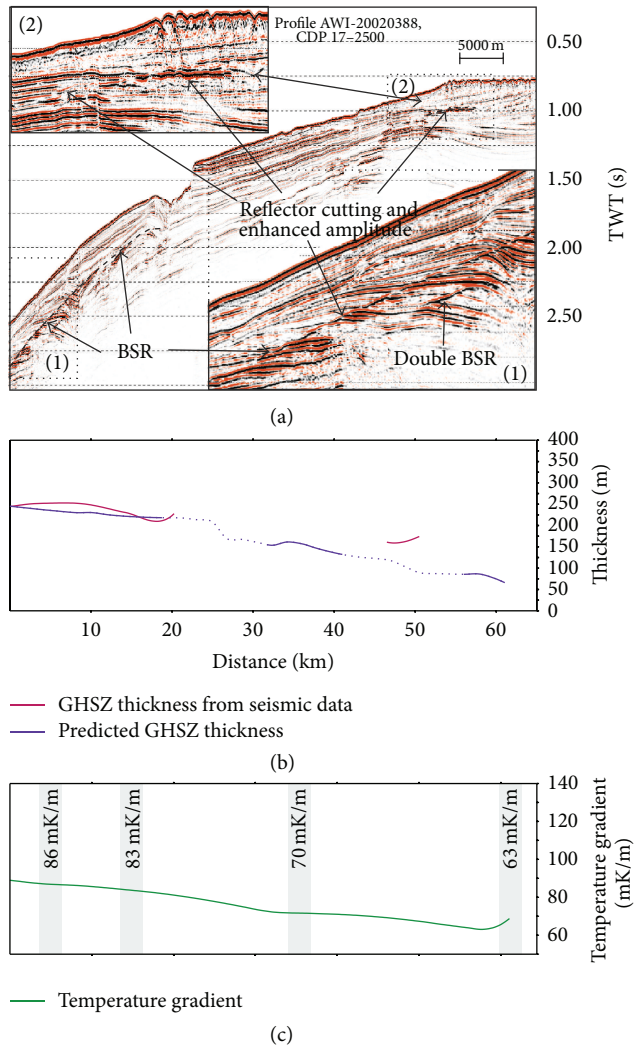

Figure 6: (a) Seismic profile AWI-20020388 (see Figure 8 for location) with BSR. Insets (1) and (2) show closeups of the BSR. (b) Interpolated GHSZ thickness along this profile is shown in pink and predicted GHSZ thickness is shown in violet. (c) Interpolated temperature gradient along this profile, grey boxes indicate heat flow measurements on that profile.

were processed in a similar way, including sorting (common depth point, hereafter CDP, and spacing 25 m), frequency filtering, velocity analysis, velocity filtering/multiple suppression, stacking (fold 40–60), and migration in time domain [32]. The success of the multiple suppression technique was limited due to the short streamer length. In addition, multibeam swath and PARASOUND sediment echo sounder data were acquired to characterize the sediment structures [30, 31, 33].

3. Results and Discussion

3.1. Temperature Gradients and Heat Flow in the Fram Strait. Figure 2 shows a map of published and new temperature gradient measurements north of 75°N. The temperature gradient values were averaged with a blockmean algorithm in order to avoid aliasing and then interpolated on a grid with a spacing of 10×10 km (Figure 3) using GMT (generic mapping tool; [34]). The new temperature gradient values fit very well to previously published values in the Fram Strait. It is obvious that high values follow the mid ocean ridges, while the old, cold continental crust beneath the shelf area is characterized by low temperature gradients. For the young oceanic crust an empirical equation between heat flow and crustal age (in million years) was proposed by Sundvor et al. [20]:

$$\text{heat flow} = \frac{420}{\sqrt{\text{age}}}. \quad (1)$$

Figure 3 shows the interpolated temperature gradient together with ages from magnetic spreading anomalies interpreted by Engen et al. [28]. Magnetic anomalies (chrons) are

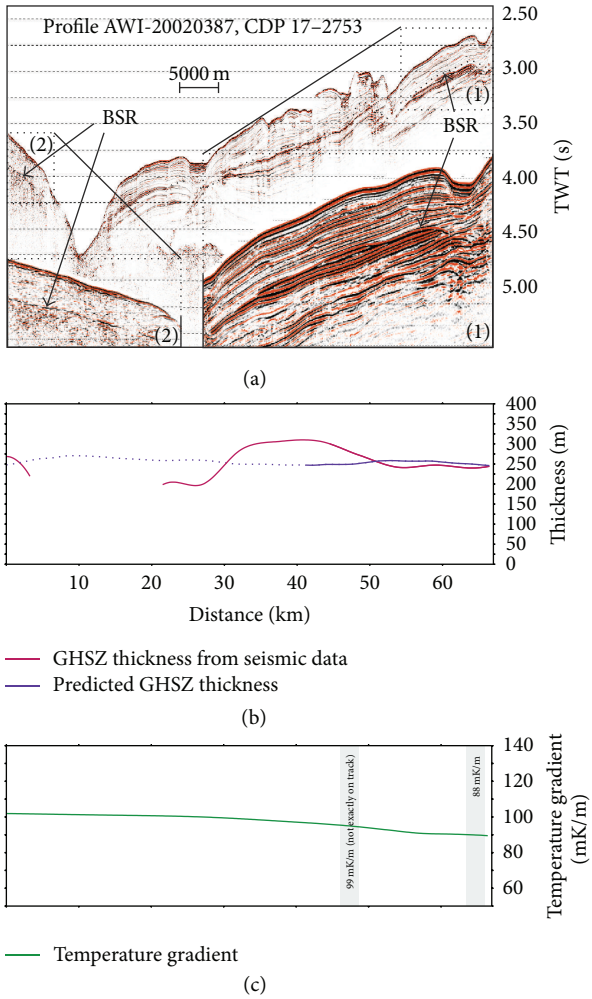

FIGURE 7: (a) Seismic profile AWI-20020387 (see Figure 8 for location) with BSR. Inlets (1) and (2) show closeups of the BSR. (b) Interpolated GHSZ thickness along this profile is shown in pink and predicted GHSZ thickness is shown in violet. Between km 30 and 50, the uppermost sediments are slightly disturbed. (c) Interpolated temperature gradient along this profile, grey boxes indicate heat flow measurements on that profile.

numbered and dated (time scale of Cande and Kent [35]). Chrons C2An.1n, C5n.1n, and C7n.1n are displayed together with the temperature gradient in Figure 3. The ages are used to calculate the heat flow and from that the temperature gradient. A thermal conductivity of 1.16 W/(m K) was used for this calculation, which is a mean for the closer research area [20]. As already observed by Sundvor et al. [20], there are some areas along the continental slope, which show anomalous high heat flow/temperature gradient values (Figure 3). One of these anomalous areas is located directly north-west of Spitsbergen at about 80°N. Another one covers the western slope of the Yermak Plateau between 81°N and 82°N. Sundvor et al. [20] speculated that these anomalies may be caused by seeping mud, fluid, and/or gas.

3.2. BSR—Theoretical Depth and Distribution. Figure 4 shows a map of the predicted GHSZ thickness. The thickness h_S was calculated solving nonlinear equation (2); further details can be found in Pulm [36]:

$$\frac{1}{1000} \times e^{a+b/(T_W+h_S \times \mathrm{GH})} - \rho_S \times g \times h_S = \rho_W \times g \times h_W - \frac{1}{1000} \times e^{a+b/T_W}, \quad (2)$$

where GH is the geothermal gradient, T_W is bottom water temperature, h_S is thickness of overlying sediments, h_W is water depth, ρ_S and ρ_W are density of sediments and water, respectively. The grid was calculated with a 10 km spacing from the temperature gradient grid (Figure 3) and water depths from the IBCAO bathymetry grid [37] for each data point, where temperature gradient values were available. The other parameters required for a GHSZ thickness prediction were taken constant for the whole area. For our calculations we used the constant values for (a) 1020 kg/m^3 density of the water, (b) 9.81 m/s^2 as gravitational acceleration, and (c) 1800 kg/m^3 as sediment bulk density averaged from the upper 100 m densities of the ODP cores in the Fram Strait [38]. To convert two-way travel time to depth below seafloor we used a sonic velocity of 1800 m/s. In general, the estimated GHSZ in our research area shows thicknesses between 50 m and 300 m (Figure 4). The filled dark blue areas indicate that gas hydrates are not stable within the shelf sediments. This is the case for water depths less than 280 m, with the assumption that bottom water temperature is 2°C for all areas shallower than 500 m. The water depth in which the BSR pinches out at the seafloor is highly sensitive to changes in bottom water temperature. Therefore, 1 K temperature increase or decrease would shift the depth where the phase boundary intersects the sea floor to 316 m or 252, respectively. Please note that the calculated depth indicates, where a BSR might occur, if free gas and overlying gas hydrates are present. It needs to be kept in mind that this theoretical map of GHSZ thickness does not take all variables (gas composition, pore water composition, and pore pressure conditions; see [1]) into account and thus predicted values can differ from the actual thickness. Furthermore, its quality is limited by the sparse distribution of heat flow data.

3.3. Gas Hydrates in the Seismic Data Offshore Spitsbergen/Svalbard. Indications of gas hydrates and free gas at the Spitsbergen slope and on Yermak Plateau are observed on several seismic profiles. We show profiles AWI-20040050, AWI-20020387 and AWI-20020388 as examples (Figures 5 to 7). The locations of these profiles are shown in Figure 8. The BSR depths along all seismic profiles along the western Yermak Plateau slope were gridded and extrapolated with a 2 km resolution on a radius of 5 km around each data point (Figure 8). The features, which characterise the BSR in those seismic profiles, are phase-reversals, reflector cutting horizons, sudden increases in amplitudes, and increases in wavelength (Figure 5(a)). A BSR is also commonly marked by a decrease in P-wave velocity below the GHSZ [39]. This, however, could not be validated along our seismic profiles, because the velocity analyses for the seismic data do not resolve shallow velocity variations in that detail. It has to

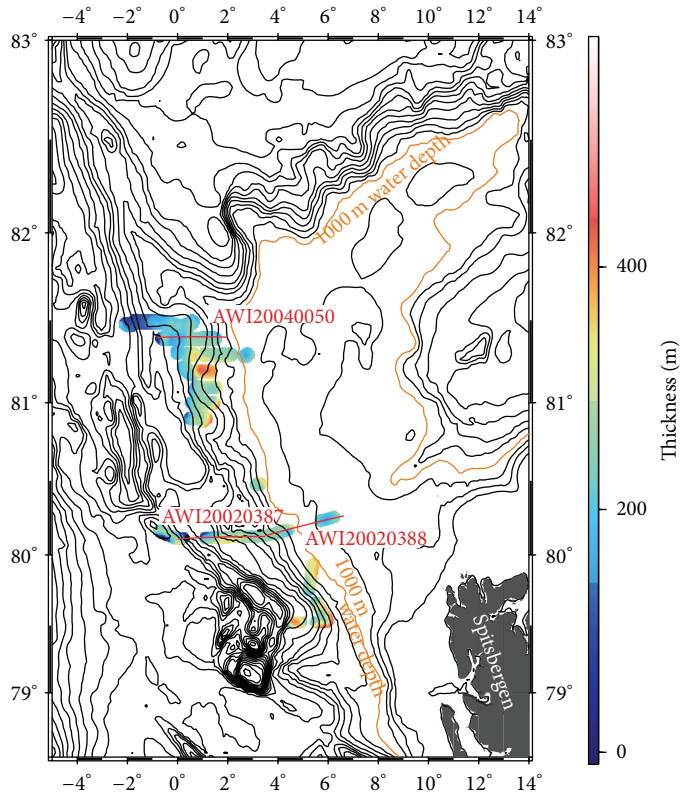

Figure 8: Map of the BSR depth (thickness of GHSZ) in the sediments along the western slope of the Yermak Plateau extracted from the available seismic profiles. Red lines indicate position of those seismic profiles described in the text and in Figures 5 to 7. Contour line spacing of isobaths is 250 m.

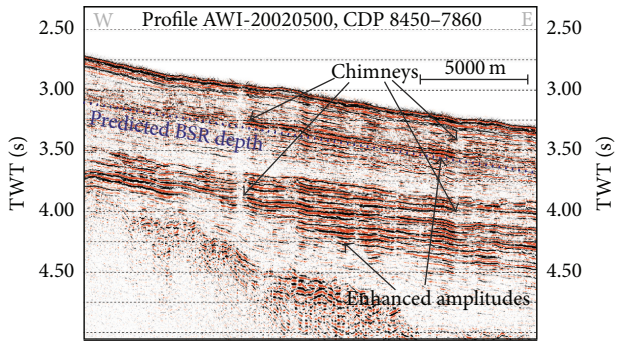

Figure 9: Part of seismic profile AWI-20020500 from the lower continental rise off East Greenland. Gas chimneys and reflectors with an increased amplitude, as well as the theoretical depth of the BSR, are marked.

be kept in mind that due to severe ice conditions during data acquisition only a short streamer could be used and shot-receiver geometry might be distorted. The other BSR characteristics are shown in the closeups of Figures 5(a) to 7(a). They all show an increase in amplitude, reflector cutting, and sea floor mimicking reflectors. Evidence for free gas within the sediment column is bright spots in the seismic data in profiles AWI-20040050 and AWI-20020388 (Figures 5(a) and 6(a)).

Figures 5(b) to 7(b) display the predicted thickness of the GHSZ, the thickness of the GHSZ according to the seismic data and the temperature gradient along the tracks as extracted from our calculated grids (Figures 3, 4, and 8). The GHSZ in profile AWI-20040050 (Figure 5) is thicker on the upper (200 to 275 m) than on the lower slope (150 to 225 m). The theoretical GHSZ thickness, however, decreases upslope (Figure 5(b)). The predicted values fit best with those measured in the lower part. In the area, where our data fit best a heat flow measurement was taken by Sundvor et al. [20]. The temperature gradient at that point is as high as 131 mK/m (Figure 5(c)). Please keep in mind that we applied a constant thermal conductivity of 1 mW/m^2 and that it might vary from 0.8 to 1.2 mW/m^2, according to Sundvor et al. [20]. This actually introduces an uncertainty to our calculations of 20%. The BSR is most pronounced on the slope at depths between 1.75 and 2.75 s twoway travel time (km 25 to 40). So far, we did not observe any indications for active seepage in the area.

Profile AWI-20020388 (Figure 6) runs across the western slope of the Yermak Plateau. Between profile kilometres 0 and 20, observed and synthetic GHSZ thicknesses concur well (250 to 200 m). The difference between both is less than 10%. The GHSZ in the upper part (Figure 6(a); km 45 to 55,

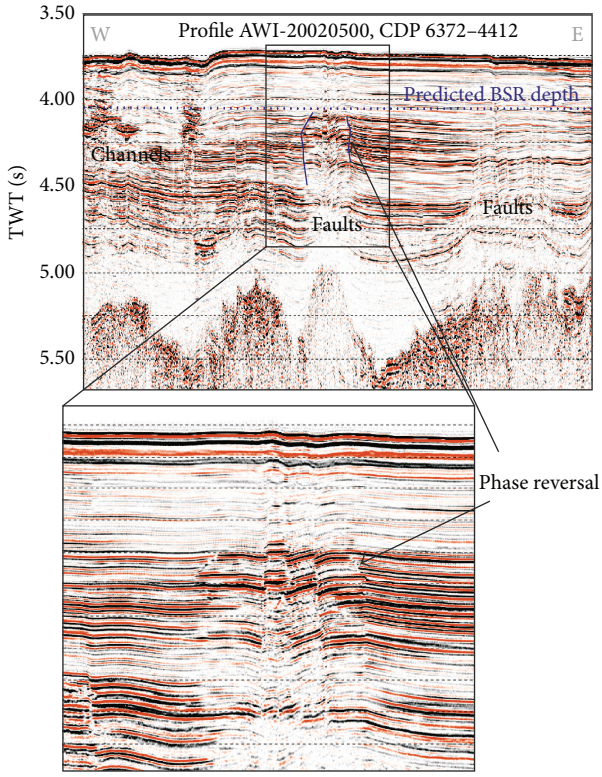

FIGURE 10: This figure shows faults along profile AWI-20020500. The theoretical depth of the BSR is at about 275 m (blue line) applying a measured temperature gradient of 105 mK/m.

inset 2) as indicated by seismic data seems to be 50 m too thick (thickness 150 m). In the western part of the profile, a second BSR occurs approximately 100 m below the upper one. Double BSRs were previously described by various authors [40–42]. The predicted GHSZ thickness along this profile (Figure 6(b)) fits much better to the observations than along profile AWI20040050 (Figure 5(b)). This can be explained by a denser coverage of reliable heat flow measurements in the vicinity of the profile, which allow to calculate a GHSZ thickness with a higher accuracy. The BSR imaged in Figure 6(a) in inset (2) (km 45 to 50), however, seems to be too deep. It, thus, might just be a bright spot, which indicates gas enriched sediments. The layers in the lower left corner of Figure 6 (inset 2) also show increased amplitudes, which points to the existence of free gas.

Remarkable along this profile is a slide scar at km 20 to 25 (Figure 6(a)). The height of the scar roughly coincides with the depth of the BSR in the sediment away from the scar. This could be an indication for a causal link between the occurrence of the gas hydrates and the slope instability. The slide scar is already filled with contouritic sediments and, thus, has an unknown age.

Profile AWI-20020387 (Figure 7) starts in the Spitsbergen Fracture Zone (km 10) and continues towards the rise of the Yermak Plateau. Along the profile the misfit between theoretical GHSZ thickness and those from the seismic data (200 to 300 m) differs up to ±50 m. At the eastern most part (Figure 7, inset 1) the fit is best. This is also the position of the only existing temperature gradient measurement directly on the profile. The area within 10 km east of the fracture zone shows a theoretical GHSZ thickness, which is 50 m too thick. The theoretical temperature gradient as calculated from the measured BSR depth would be 140 mK/m, which is 40 mK/m higher than interpolated from existing temperature gradient measurements (Figure 3). One explanation for the misfit between km 20 and 50 could be a badly interpolated temperature gradient, which might be plausible in the vicinity of the Spitsbergen Fracture Zone. Another reason for the observed discrepancies might be that the disturbed uppermost sediments imaged by the seismic data are not under thermal equilibrium conditions.

At some sites the predicted BSR matches the real BSR, at others they show significant differences. The prediction of the BSR depth mainly lacks two points. On the one hand the prediction method itself is not perfectly precise. Several assumptions are made, which restricts the quality of the results. On the other hand, the input data for the variables used for the calculations are fairly uncertain. The coverage of the heat flow data and conductivity measurements is very poor and, thus, inter- and extrapolation might result in large errors. Furthermore, areas with a GHSZ that is thinner than that proposed by the temperature gradient might be under the influence of migrating warm fluids as observed by Zühlsdorff et al. [43] on the continental slope off Vancouver Island, Canada.

3.4. Gas in the Seismic Data off Northeast Greenland. Along the East Greenland continental margin the GHSZ is predicted to be rather thick (Figure 4). This is due to significantly lower temperature gradients compared to gradients along the western Svalbard continental slope. No clear BSR could be identified in the analysed seismic data off East Greenland (Figures 9 and 10). This can be due to several reasons. A simple explanation is the absence of a BSR-forming process such as the existence of a boundary between gas hydrates and free gas below. There could be gas hydrates nonetheless, but the prevailing seismic facies is characterized by more or less horizontal and parallel reflections, which makes it difficult to identify any hydrate-related BSR. Also it is not possible to judge, whether one of the many local enhanced seismic amplitudes or seismic phase variations is caused by the transition between GHSZ and free gas. But, there are other features than a BSR, which point to the presence of free gas within the sedimentary basins. Figure 9 shows part of seismic profile AWI-20020500 from the lower continental slope. Amplitude variations in the seismic data are obvious. There are vertically elongated structures with remarkably weak amplitudes. Those might be chimneys, paths for fluids, gases, and muds. In the vicinity of the chimneys, the amplitudes are somewhat higher. These amplitudes anomalies might be caused by gas, which is entrapped in the sediment layers. Blanking zones like in the described chimneys were identified as focused fluid flow paths [44].

Indications for free gas can also be found further east in the abyssal plain (Figure 10), where gas or fluid seems to rise

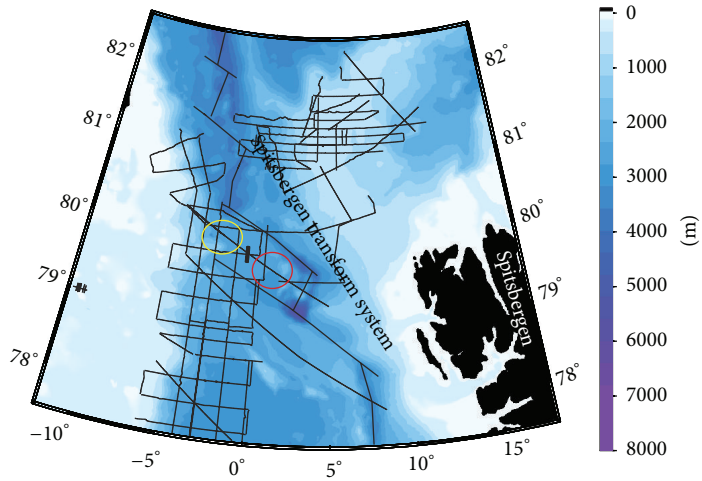

Figure 11: The figure shows the Spitsbergen Transform System after Engen (2005) [29] with the IBCAO bathymetry and seismic profiles used in this study. The red circle marks the area where faults are the main gas/fluid pathways, and the yellow circle marks the area in which the upward migration of gas seems to be related to chimneys (causing blanking zones).

along vertical fault systems. Amplitudes are stronger in the immediate neighbourhood of the faults that reach up to the seafloor in most cases. The high amplitude reflections also show phase reversals in a depth of 4.0–4.5 s TWT, which is another indication of free gas (Figure 10). A theoretical BSR depth is marked in Figure 10. Phase reversals and amplitude variations are observed below that zone. Free gas probably migrates through the fault pathways and the neighbouring sediment becomes enriched in gas, which results in higher amplitudes and phase reversals. The faults and chimneys can be found on some more profiles. Areas of their occurrence are marked in Figure 11. The seismic profiles, on which the faults are visible, are located between two transform faults (Figure 11). Therefore, we propose a tectonic origin of the faults.

3.5. Differences between the Svalbard and East Greenland Continental Slope Areas. Gas hydrates are present in the sediments of the continental slope off western Svalbard and the western Yermak Plateau margin, which are deposited under the influence of bottom currents. In general, GHSZ thins downslope along the western Yermak Plateau slope. GHSZ thickness is predicted to be very thin along the active rift zones in the Fram Strait because of high heat flow there. Along the western Yermak Plateau slope and in the adjacent deep sea basin, there is seismic evidence for the occurrence of gas hydrates. BSRs are imaged along seismic profiles AWI-20020388 and AWI-20040050. Sediments in the more northern area (Profile AWI-20040050, Figure 5), however, might not contain as much gas as sediments further south, because there the BSR and relative amplitude anomalies are much stronger in the southern area.

The GHSZ for the NE Greenland margin is, according to the prediction from heat flow data, thicker than along the western Svalbard and Yermak Plateau slopes. This, however, cannot be confirmed by the seismic data; no BSR could be identified in the analysed data. The absence of a BSR could be explained by a lack of organic material in the sediment producing significant amounts of gas. Even if there is organic gas, it needs to occur in a certain amount in order to occur as free gas below the GHSZ and to cause a BSR. Existing gas migrates along near-vertical pathways. Much more chimneys and faults, which are pathways for gas, are visible on existing seismic data in the vicinity of the East Greenland margin than offshore Svalbard.

The gas did not form in situ, since the total organic carbon (TOC) is lowest in the upper most part of the sediment [45]. At ODP site 909 TOC values vary from 0.2% to 1.4% in Pleistocene sediments, while Pliocene and upper Miocene sediments show values between 0.8% and 1.7%. Connell et al. [45] also state that the Fram Strait region has been void of almost any biogenic sedimentation from the late early Miocene to present. Thus, the gas, which is now trapped in gas hydrates along the slope, must have migrated through the sediment succession. No pockmarks or other traces of focused seepages could be identified on the Yermak Plateau so far. Damm et al. [46] describe micro-seepage structures further south between 76°30′N and 78°N along the western Svalbard continental margin, and the same authors also conclude from an increased methane content in the water column that methane is presently discharged at the seafloor. There is also a strong difference in sediment input between W Svalbard and NE Greenland. The western Svalbard continental slope receives terrigenous input from the islands and from the Barents shelf, on which coal layers and other organic rich layers exist, which are then transported north with the West Spitsbergen current. In contrast, the East Greenland current does not carry any significant material (pers. com. U. Schauer 2010) and, hence, no organic content either.

Another methane source might be the serpentinization of unroofed upper mantle [47, 48] in the ultra-slow spreading Lena Trough and Molloy Deep and associated fracture zones in the Fram Strait. Serpentinization of peridotites results in

elevated heat flow and produces methane (via hydrogen). This gas might migrate through the sediments to form hydrates close to the seafloor.

4. Conclusions

The temperature gradients along the West Svalbard continental margin show two areas with elevated heat flow. Overall, the temperature gradient on the southwestern Yermak Plateau slope is about 75 mK/m. The range of heat flow typical for the crust below the shelf areas is 50 to 75 m/Wm^2 [20]. Thus, the observed temperature gradient lies in the upper range of what would be expected. Along seismic profiles, a bottom simulating reflector (BSR), which marks the lower base of the gas hydrate stability zone (GHSZ), was identified. The depth of the BSR was predicted on the basis of measured temperature gradient values. The fit between predicted and measured BSR depth is excellent at locations where temperature gradient measurements exist.

The source of the gas, which escapes through the chimneys at the East Greenland continental rise around 80°N, is located in the deeper sedimentary succession. The total organic content of the sediments in the Fram Strait decreased significantly since the early Miocene, which makes a formation of organic gas in the lower sedimentary succession and a subsequent migration through the sedimentary cover likely.

The abyssal plain of the Fram Strait is mainly underlain by oceanic crust and unroofed uppermost mantle peridotites. The observed temperature gradients are remarkably high along the spreading ridges. They partly exceed 200 mK/m, which fits to an expected temperature gradient of >100 mK/m [20]. Fluids and gas migrate through faults, which are most probably of tectonic origin. Serpentinization of tectonically unroofed peridotites might represent a potential source of methane.

Our study shows that the well-studied gas hydrate province along the West Svalbard continental slope extends much farther north along the slope of the western Yermak Plateau. So far, no recent seepages were observed indicating active venting.

Conflict of Interests

The authors declare that there is no conflict of interests regarding the publication of this paper.

Acknowledgments

The authors thank Captain Schwarze of RV POLARSTERN and the entire crew of ARK-XXIV/3. Furthermore, they are grateful to H. Villinger and N. Kaul for providing the heat flow probe and know-how of heat flow processing. They thank all people who collected seismic data over the past decades in sometimes heavy ice conditions to make this work possible. Maps were generated using the Generic Mapping Tools software [34]. The authors are grateful to Academic Editor M. Giustiniani and two anonymous reviewers.

References

[1] U. Tinivella and M. Giustiniani, "Variations in BSR depth due to gas hydrate stability versus pore pressure," *Global and Planetary Change*, vol. 100, pp. 119–128, 2013.

[2] E. D. Sloan, *Clathrate Hydrates of Natural Gases*, Marcel Dekker, 1998.

[3] B. Ferre, J. Mienert, and T. Feseker, "Ocean temperature variability for the past 60 years on the Norwegian-Svalbard margin influences gas hydrate stability on human time scales," *Journal of Geophysical Research C*, vol. 117, no. 10, 2012.

[4] M. F. Nixon and J. L. H. Grozic, "A simple model for submarine slope stability analysis with gas hydrates," *Norwegian Journal of Geology*, vol. 86, no. 3, pp. 309–316, 2006.

[5] D. Winkelmann, W. Jokat, F. Niessen, R. Stein, and W. Winkler, "Age and extent of the Yermak Slide north of Spitsbergen, Arctic Ocean," *Geochemistry, Geophysics, Geosystems*, vol. 7, no. 6, Article ID Q06007, 2006.

[6] D. Winkelmann, W. Geissler, J. Schneider, and R. Stein, "Dynamics and timing of the Hinlopen/Yermak Megaslide north of Spitsbergen, Arctic Ocean," *Marine Geology*, vol. 250, no. 1-2, pp. 34–50, 2008.

[7] S. Hustoft, S. Bünz, J. Mienert, and S. Chand, "Gas hydrate reservoir and active methane-venting province in sediments on < 20 Ma young oceanic crust in the Fram Strait, offshore NW-Svalbard," *Earth and Planetary Science Letters*, vol. 284, no. 1-2, pp. 12–24, 2009.

[8] T. Gentz, E. Damm, J. S. von Deimling, S. Mau, D. F. McGinnis, and M. Schlüter, "A water column study of methane around gas flares located at the Wets Spitsbergen continental margin," *Continental Shelf Research*, vol. 72, pp. 107–118, 2014.

[9] A. G. Judd and M. Hovland, "The evidence of shallow gas in marine sediments," *Continental Shelf Research*, vol. 12, no. 10, pp. 1081–1095, 1992.

[10] P. R. Vogt, J. Gardner, and K. Crane, "The Norwegian-Barents-Svalbard (NBS) continental margin: introducing a natural laboratory of mass wasting, hydrates, and ascent of sediment, pore water, and methane," *Geo-Marine Letters*, vol. 19, no. 1-2, pp. 2–21, 1999.

[11] G. K. Westbrook, K. E. Thatcher, E. J. Rohling et al., "Escape of methane gas from the seabed along the West Spitsbergen continental margin," *Geophysical Research Letters*, vol. 36, no. 15, Article ID L15608, 2009.

[12] J. Mienert, M. Vanneste, S. Bünz, K. Andreassen, H. Haflidason, and H. P. Sejrup, "Ocean warming and gas hydrate stability on the mid-Norwegian margin at the Storegga Slide," *Marine and Petroleum Geology*, vol. 22, no. 1-2, pp. 233–244, 2005.

[13] S. Chand and T. A. Minshull, "Seismic constraints on the effects of gas hydrate on sediment physical properties and fluid flow: a review," *Geofluids*, vol. 3, no. 4, pp. 275–289, 2003.

[14] M. Vanneste, S. Guidard, and J. Mienert, "Bottom-simulating reflections and geothermal gradients across the Western Svalbard margin," *Terra Nova*, vol. 17, no. 6, pp. 510–516, 2005.

[15] R. R. Haacke, G. K. Westbrook, and M. S. Riley, "Controls on the formation and stability of gas hydrate-related bottom-simulating reflectors (BSRs): a case study from the west Svalbard continental slope," *Journal of Geophysical Research B*, vol. 113, no. 5, 2008.

[16] J. Posewang and J. Mienert, "High-resolution seismic studies of gas hydrates west of Svalbard," *Geo-Marine Letters*, vol. 19, no. 1-2, pp. 150–156, 1999.

[17] A. Chabert, T. A. Minshull, G. K. Westbrook, C. Berndt, K. E. Thatcher, and S. Sarkar, "Characterization of a stratigraphically constrained gas hydrate system along the western continental margin of Svalbard from ocean bottom seismometer data," *Journal of Geophysical Research B*, vol. 116, no. 12, 2011.

[18] H. N. Pollack, S. J. Hurter, and J. R. Johnson, "Heat flow from the earth's interior: analysis of the global data set," *Reviews of Geophysics*, vol. 31, no. 3, pp. 267–280, 1993.

[19] IHFC, *Global Heat Flow Database*, International Heat Flow Commission, 2010, www.heatflow.und.edu.

[20] E. Sundvor, O. Eldholm, T. P. Gladczenko, and S. Planke, "Norwegian-Greenland Sea thermal field," *Geological Society*, vol. 167, pp. 397–410, 2000.

[21] W. Jokat, "The expedition of the research vessel " Polarstern" to the Arctic in 2009 (ARK-XXIV/3)," Scientific Cruise Report 615, Berichte zur Polar- und Meeresforschung, 2010.

[22] D. Berger and W. Jokat, "A seismic study along the East Greenland margin from 72°N to 77°N," *Geophysical Journal International*, vol. 174, no. 2, pp. 733–748, 2008.

[23] D. Berger and W. Jokat, "Sediment deposition in the northern basins of the North Atlantic and characteristic variations in shelf sedimentation along the East Greenland margin," *Marine and Petroleum Geology*, vol. 26, no. 8, pp. 1321–1337, 2009.

[24] T. Hermann and W. Jokat, "Crustal structures of the Boreas Basin and the Knipovich Ridge, North Atlantic," *Geophysical Journal International*, vol. 193, no. 3, pp. 1399–1414, 2013.

[25] H. Villinger and E. E. Davis, "A new reduction algorithm for marine heat flow measurements," *Journal of Geophysical Research B*, vol. 92, no. 12, pp. 12846–12856, 1987.

[26] M. Urlaub, M. C. Schmidt-Aursch, W. Jokat, and N. Kaul, "Gravity crustal models and heat flow measurements for the Eurasia Basin, Arctic Ocean," *Marine Geophysical Researches*, vol. 30, no. 4, pp. 277–292, 2009.

[27] E. Fahrbach, J. Meincke, S. Østerhus et al., "Direct measurements of volume transports through Fram Strait," *Polar Research*, vol. 20, no. 2, pp. 217–224, 2001.

[28] Ø. Engen, J. I. Faleide, and T. K. Dyreng, "Opening of the Fram Strait Gateway: a review of plate tectonic constraints," *Tectonophysics*, vol. 450, no. 1-4, pp. 51–69, 2008.

[29] Ø. Engen, *Evolution of High Arctic Ocean basins and bontinental margins, [Ph.D. thesis]*, University of Oslo, 2005.

[30] W. Jokat, "Die expedition 13 ARKTIS XVIII/2 mit FS Polarstern, 2002," Scientific Cruise Report 449, Berichte zur Polar- und Meeresforschung, 2003.

[31] R. Stein, "Arctic expedition ARK-XX/3 of RV "Polarstern" in 2004: Fram Strait, Yermak Plateau and East Greenland Continental Margin," Scientific Cruise Report 517, Berichte zur Polar- und Meeresforschung, 2005.

[32] W. H. Geissler, W. Jokat, and H. Brekke, "The Yermak Plateau in the Arctic Ocean in the light of reflection seismic data-implication for its tectonic and sedimentary evolution," *Geophysical Journal International*, vol. 187, no. 3, pp. 1334–1362, 2011.

[33] A. C. Gebhardt, W. H. Geissler, J. Matthiessen, and W. Jokat, "Changes in current patterns in the Fram Strait at the Pliocene/Pleistocene boundary," *Quaternary Science Reviews*, 2013.

[34] P. Wessel and W. H. F. Smith, "New improved version of generic mapping tools released," *Eos, Transactions American Geophysical Union*, vol. 79, no. 47, 579 pages, 1998.

[35] S. C. Cande and D. V. Kent, "Revised calibration of the geomagnetic polarity timescale for the late Cretaceous and Cenozoic," *Journal of Geophysical Research*, vol. 100, no. 4, pp. 6093–6095, 1995.

[36] P. Pulm, *Sedimentation processes in the Northern Fram Strait since Early Miocene [Diploma thesis]*, Fakultät für Mathematik, Informatik und Naturwissenschaften. University of Hamburg, Hamburg, Germany, 2010.

[37] M. Jakobsson, R. Macnab, L. Mayer et al., "An improved bathymetric portrayal of the Arctic Ocean: implications for ocean modeling and geological, geophysical and oceanographic analyses," *Geophysical Research Letters*, vol. 35, no. 7, Article ID L07602, 2008.

[38] F. R. Rack, J. Bloemendal, T. C. W. Wolf-Welling et al., "Development of physical properties relationships, interhole composite depth profiles, and sedimentologic ground truthing of multi-sensor core measurements: a synthesis of results," in *Proceedings of the Ocean Drilling Program, Scientific Results*, J. Thiede, A. M. Myre, J. V. Firth, G. L. Johnson, and W. F. Ruddiman, Eds., vol. 151, pp. 595–626, National Science Foundation and Joint Oceanographic institutions, 1996.

[39] G. L. Netzeband, C. P. Hübscher, D. Gajewski, J. W. G. Grobys, and J. Bialas, "Seismic velocities from the Yaquina Forearc Basin Off Peru: evidence for free gas within the gas hydrate stability zone," *International Journal of Earth Sciences*, vol. 94, no. 3, pp. 420–432, 2005.

[40] J.-P. Foucher, H. Nouzé, and P. Henry, "Observation and tentative interpretation of a double BSR on the Nankai slope," *Marine Geology*, vol. 187, no. 1-2, pp. 161–175, 2002.

[41] C. Berndt, S. Bünz, T. Clayton, J. Mienert, and M. Saunders, "Seismic character of bottom simulating reflectors: examples from the mid-Norwegian margin," *Marine and Petroleum Geology*, vol. 21, no. 6, pp. 723–733, 2004.

[42] G. K. Westbrook, S. Chand, G. Rossi et al., "Estimation of gas hydrate concentration from multi-component seismic data at sites on the continental margins of NW Svalbard and the Storegga region of Norway," *Marine and Petroleum Geology*, vol. 25, no. 8, pp. 744–758, 2008.

[43] L. Zühlsdorff, V. Spieß, C. Hübscher, H. Villinger, and A. Rosenberger, "Implications for focused fluid transport at the northern Cascadia accretionary prism from a correlation between BSR occurrence and near-sea-floor reflectivity anomalies imaged in a multi-frequency seismic data set," *International Journal of Earth Sciences*, vol. 88, no. 4, pp. 655–667, 2000.

[44] L. Zühlsdorff and V. Spieß, "Three-dimensional seismic characterization of a venting site reveals compelling indications of natural hydraulic fracturing," *Geology*, vol. 32, no. 2, pp. 101–104, 2004.

[45] S. O. Connell, T. C. Wolf-Welling, M. Cremer, and R. Stein, "Neogene paleoceanography and paleoclimate history from Fram Strait: changes in accumulation rates," in *Proceedings of the Ocean Drilling Program, Scientific Results*, J. Thiede, A. M. Myhre, J. V. Firth, G. L. Johnson, and W. F. Ruddiman, Eds., vol. 151, pp. 569–582, National Science Foundation and Joint Oceanographic institutions, 1996.

[46] E. Damm, A. Mackensen, G. Budéus, E. Faber, and C. Hanfland, "Pathways of methane in seawater: plume spreading in an Arctic shelf environment (SW-Spitsbergen)," *Continental Shelf Research*, vol. 25, no. 12-13, pp. 1453–1472, 2005.

[47] N. H. Sleep, A. Meibom, T. Fridriksson, R. G. Coleman, and D. K. Bird, "H2-rich fluids from serpentinization: Geochemical and biotic implications," *Proceedings of the National Academy of Sciences of the United States of America*, vol. 101, no. 35, pp. 12818–12823, 2004.

[48] A. Rajan, J. Mienert, S. Bünz, and S. Chand, "Potential serpentinization, degassing, and gas hydrate formation at a young (<20 Ma) sedimented ocean crust of the Arctic Ocean ridge system," *Journal of Geophysical Research B*, vol. 117, no. 3, Article ID B03102, 2012.